Ecotoxicology and Environmental Safety 303 (2025) 118830

Contents lists available at ScienceDirect

Ecotoxicology and Environmental Safety

journal homepage: www.elsevier.com/locate/ecoenv

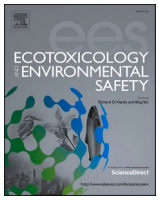

Mechanistic insights into fluoride-induced reproductive toxicity in female ovine animals: Mitochondrial dysfunction and ER stress-driven apoptosis in ovine granulosa cells

Tian Ma [a], Didi Jiang [a], Wanruo Liu [a], Zongshuai Li [b], Kun Gao [c], Yong Zhang [a,*]

[a] College of Veterinary Medicine, Gansu Agricultural University, Lanzhou, China
[b] College of Life Science, Baicheng Normal University, Baicheng, China
[c] College of Life Science and Technology, Gansu Agricultural University, Lanzhou, China

ARTICLE INFO

Edited by Dr Yong Liang

Keywords:
Fluoride
Ovine granulosa cells
Oxidative stress
Endoplasmic reticulum stress

ABSTRACT

The aim of this study was to investigate the effects of fluoride on ovine granulosa cells (GCs). GCs were treated with NaF to assess the effects of fluoride exposure on their morphology and function. Reactive oxygen species (ROS) level, mitochondrial membrane potential (MMP), and malondialdehyde (MDA) and glutathione (GSH) contents were determined. The expression of genes and proteins related to oxidative stress and endoplasmic reticulum stress (ERS) was examined. Additionally, RNA sequencing (RNA-Seq) and molecular biological techniques were used to elucidate the potential mechanisms underlying fluoride-induced damage to GCs. Fluoride treatment generated oxidative stress in cells, resulting in the overproduction of intracellular ROS, accumulation of lipid peroxidation products, decreased cellular antioxidant enzyme activities, and increased cellular damage. Treatment with N-acetylcysteine (NAC) effectively increased the fluoride-induced decrease in catalase (CAT), superoxide dismutase 1 (SOD1), and glutathione peroxidase 1 (GPX1) expression ($P < 0.01$, $P < 0.05$). Fluoride exposure induced ERS in GCs. The mRNA expression of *BIP, PERK, ATF4, ATF6, CHOP, GADD34, ERN1,* and *XBP1* significantly increase under NaF treatment ($P < 0.01$). Binding immunoglobulin protein (BIP), protein kinase R-like endoplasmic reticulum kinase (PERK), and activating transcription factor 6 (ATF6) expression significantly increased ($P < 0.01$). The ERS inhibitor GSK2656157 reduced the expression of BIP, PERK, and ATF6 ($P < 0.01$, $P < 0.05$). RNA-Seq analysis showed that the expression of genes associated with ERS was activated; genes associated with oxidative stress were repressed; and Environmental Information Processing, Genetic Information Processing, Metabolism, Cellular Processes, and Human Disease pathways were activated. This study provides a deep understanding of fluoride-induced reproductive toxicity and offers potential strategies to mitigate its effects to protect animal and human reproductive health.

1. Introduction

Fluoride is a widespread environmental pollutant, which has been extensively studied because of its toxic effects on various biological systems. Fluoride poisoning is a public health concern with significant global impact. With ongoing developments of industry and agriculture, increasing amounts of fluoride compounds enter the environment and human living areas through drinking water, pesticides, and fungicides. In regions with high fluoride pollution, excessive long-term fluoride intake negatively affects tissues and organs. Notably, while fluoride poisoning primarily affects teeth and bones, it can also impact non-skeletal organs. Recent studies have gradually shifted toward non-skeletal effects, particularly those of the reproductive system (Vasisth et al., 2024).

Excessive accumulation of fluoride in the body impairs the physiological functions of various organs such as the liver, kidneys, heart, intestines, testes, ovaries, and other tissues (Li et al., 2021; Wang et al., 2023). Fluoride can lead to disorders in sex hormone levels and destruction of blood-testicular barriers, interfere with the body's immune function and sperm production, trigger sperm dysfunction in the testicles, reduce the quantity and quality of sperm (Pramanik and Saha, 2017; Suzuki et al., 2015), cause inflammatory responses and oxidative stress, and activate cell autophagy, necrosis, and apoptosis, ultimately causing male reproductive dysfunction (Öncü et al., 2007; Sun et al.,

* Corresponding author.
E-mail address: zhangyong@gsau.edu.cn (Y. Zhang).

https://doi.org/10.1016/j.ecoenv.2025.118830
Received 11 June 2025; Received in revised form 30 July 2025; Accepted 5 August 2025
Available online 8 August 2025

2016). Ultrastructural analysis of mouse testicular tissue has revealed that fluoride exposure damages mitochondria of testicular germ, Sertoli, and Leydig cells, and induces autophagy. The endoplasmic reticulum becomes dilated and degranulated, while the spermatogenic epithelium shows vacuolization and apoptosis (Liang et al., 2020); mitochondria exhibit swelling, with some showing ruptured or tubular cristae and condensed cytoplasm (Zhang et al., 2013). Fluoride inhibits follicular maturation and directly damages the ovaries and uterus, leading to reproductive dysfunction. Fluoride exposure causes various pathological damages to uterine epithelial cells in pregnant mice. It induces uterine epithelial damage through oxidative stress, thereby causing reproductive toxicity. Fluoride exposure increases reactive oxygen species (ROS) levels, significantly reduces glutathione (GSH), and elevates cathepsin B activity in porcine oocytes, suggesting that oxidative stress-induced damage impairs porcine reproductive cells. The intake of fluoride at high concentrations alters the structural integrity of the uterus and morphology of the ovaries, induce apoptosis, and impair oocyte maturation and hinder its development and fertilization (Liang et al., 2017; Wang et al., 2017). In addition, exposure to high fluoride concentrations leads to a reduction in pregnancy rates and litter size in female mice. Ultrastructural observations of the uterine tissue in these mice have revealed several abnormalities, including nuclear fuzziness, diminished microvilli, accumulation of lysosomes, mitochondrial vacuolization, and distended endoplasmic reticulum (Wang et al., 2017). Furthermore, oocytes exhibit spindle breakdown and chromosomal abnormalities, while the mitochondrial membrane potential decreases (Wu et al., 2022a). These findings highlight the significant detrimental effects of fluoride exposure on reproductive health at both cellular and organ levels.

Granulosa cells (GCs) exhibit favorable growth characteristics *in vitro*, thereby serving as an ideal cellular model for mechanistic studies of pollutants-induced reproductive toxicity. GCs play a pivotal role in supporting oocyte maturation and follicular development. The follicular fluid produced by GCs contains multiple factors, including estrogen, progesterone, melatonin, and inhibin, which collectively support oocyte maturation and follicular development (Cavalcanti et al., 2023; Chen et al., 2021; Richards and Pangas, 2010). Therefore, the health and function of GCs are vital for reproductive success (Laurindo et al., 2024; Spicer et al., 2025). GCs has been successfully proposed as an *in vitro* model to assess the effects of pollutants on the female ovary (Pizzo et al., 2016). Studies have shown that the major metabolites of deoxynivalenol (DON) and zearalenone (ZEA) have an effect on bovine GCs. These toxins inhibit cell proliferation and affect steroidogenesis (Pizzo et al., 2016). Treatment with fumonisin B1, DON or ZEA could inhibited Porcine GCs proliferation and steroidogenesis (Cortinovis et al., 2014). Similarly, accumulation of copper occurred in goat GCs after treatment with mycotoxin, which promoted cell apoptosis, inhibited cell proliferation and arrested cell cycle (Liu et al., 2023). Fluoride exposure induces cytotoxicity in GCs (Geng et al., 2024; Zhao et al., 2019). A study showed that NaF induced apoptosis of GCs, leading to abnormal hormone secretion and ovarian dysfunction (Geng et al., 2024). Zhao et al. showed that fluoride can damage the mitochondrial ultrastructure of GCs, reduced ATP content, increased ROS levels, and cause mitochondrial dysfunction (Zhao et al., 2018, 2019). These studies indicated that follicular GCs are sensitive to environmental pollutants and toxins, and can be used as a primary cell model to study the damage to female reproduction. Given the crucial role of GCs in follicular development and oocyte maturation, understanding the mechanisms, through which fluoride causes damage to these cells is essential for elucidating broad impacts of fluoride on reproductive health.

Ovine animals are domestically important, are widely distributed worldwide, and have significant economic value, particularly in agriculture and livestock farming. They are highly sensitive to fluoride exposure, particularly in areas with high fluoride concentrations, and often exhibit symptoms of fluoride poisoning such as dental and skeletal damage, and reduced reproductive capacity. Contaminated water and roughage are considered the primary factors that lead to fluoride poisoning in ovine animals (Srivastava and Flora, 2020; Zuo et al., 2018). Endemic fluoride poisoning causes chronic toxicity in ovine animals involving the nervous, digestive, endocrine, and reproductive systems, and also induces genotoxicity (Efe et al., 2020; Ottappilakkil et al., 2022; Rahim et al., 2022). Similarly, animals living in fluoride-polluted areas, such as cows, horses, and camels, are affected to varying degrees by fluoride toxicity (Choubisa and Choubisa, 2016).

Despite evidence demonstrating fluoride-induced reproductive toxicity in mammals, its effects on ovine granulosa cell function have not been systematically investigated. This study aimed to investigate the cytotoxic effects of fluoride on ovine granulosa cells (GCs), focusing on the roles of oxidative stress and endoplasmic reticulum stress (ERS). Building upon existing knowledge, our findings provide fundamental data for assessing the risks of fluoride exposure to ovine GCs.

2. Materials and methods

2.1. Cell culture and treatment

The method of ovary collection, in vitro cultivation of primary GCs refers to our previous research (Ma et al., 2024). GCs obtained from ovine ovaries were cultured in a mixed medium containing 10 % fetal bovine serum (FBS, BI, Kibbutz Beit Haemek, Israel) and DMEM/F-12 (Gibico, Grand Island, NY, USA) medium in an incubator (Thermo Scientific, Waltham, MA, USA) at 37 °C with 5 % CO_2. The culture medium was replaced every 24 h. After culturing, cells were exposed to different concentrations of NaF (0, 3, 3.5, and 4 mM) (Sigma-Aldrich, St. Louis, MO, USA) or in the presence and absence of 45 μM NAC/2 μM GSK2656157 (TargetMol, Boston, MA, USA) for 24 h. The concentration of the NaF was based on our previous study. Three concentration gradients below the IC_{50} were selected for this research. For different experiments, GCs were plated in 6-well or 96-well plates (Corning, NY, USA).

2.2. Hoechst 33258 staining

Apoptotic cells were identified using Hoechst 33258 staining (Boster, Wuhan, China). After discarding the culture medium, cells were rinsed three times with phosphate-buffered saline (PBS, Biosharp, Beijing, China). Subsequently, a small amount of Hoechst 33258 staining solution was applied, and the cells were incubated at room temperature for approximately 3–5 min. The staining solution was then removed, followed by three additional PBS washes (3 min each). Fluorescent images were captured directly using a fluorescence microscope (ECHO Laboratories, San Diego, CA, USA).

2.3. Scratch-wound assay

A horizontal line was drawn evenly at the bottom of a 6-well plate using a marker. Cells in the logarithmic growth phase were harvested and digested using trypsin (Gibco, Grand Island, NY, USA) to generate a single-cell suspension, which was then seeded into the 6-well plate. The following day, a pipette tip was used to create vertical scratches along the marked lines. The cells were washed 2–3 times with PBS to remove detached cells, and serum-free medium was added. Cells were photographed at regular intervals and the photographs were analyzed using ImageJ. The images were imported into ImageJ, the scratch area was selected. The initial scratch area and the scratch area at regular intervals were measured. Finally, the closed wound area (%) was calculated.

2.4. Assessment of reactive oxygen species (ROS), MDA, and glutathione (GSH) levels, and mitochondrial membrane potential

Changes in intracellular ROS were detected using a ROS assay kit. (Elabscience, Wuhan, China). Cells were washed once with serum-free

medium; an adequate volume of working solution was added to cover the cells; and cells were incubated at 37 ℃ in the dark for 45–60 min. The working solution was removed, and the cells were washed with serum-free medium twice or thrice and then directly observed and photographed using a fluorescence microscope (ECHO, San Diego, CA, USA).

Changes in mitochondrial membrane potential were detected using an MMP Assay Kit (Elabscience, Wuhan, China). JC-1 working solution was prepared by adding 1 mL JC-1 Assay Buffer to 20 μL JC-1, and 9 mL ultrapure water was added and mixed well. to prepare 1× JC-1 Assay Buffer. Cells were washed once with 1× JC-1 Assay Buffer and incubated with an appropriate amount of JC-1 working solution at 37 ℃ for 20 min. The cells were then washed once with 1× JC-1 Assay Buffer, 2 mL of cell culture medium or 1× JC-1 Assay Buffer was added, and cells were observed and photographed using a fluorescence microscope.

The GSH and MDA contents in cell homogenates were determined using GSH and MDA kits (Jiancheng Bioengineering Institute, Nanjing, China), respectively.

2.5. Transmission electron microscopy (TEM)

For electron microscopy, the culture medium was removed from the GCs, followed by trypsin digestion. The resulting cell suspension was centrifuged at low speed for 3–5 min. The supernatant was discarded, and the cells were fixed with electron microscopy fixative (Servicebio, Wuhan, China) that was, pre-warmed to room temperature. The cell clumps were gently dispersed and resuspended, fixed at room temperature in the dark for 30 min, and then stored at 4 ℃. Random fields of view were selected and observed under a transmission electron microscope (Hitachi HT7700, Tokyo, Japan).

2.6. Quantitative real-time polymerase chain reaction (qRT-PCR)

Total RNA was extracted from the collected cells using the Total RNA Extraction Reagent (TRIgent) (Mei5bio, Beijing, China), following the manufacturer's instructions. cDNA synthesis was carried out using the Transcriptor First Strand cDNA Synthesis Kit (Thermo Fisher Scientific, Waltham, MA, USA). The primer sequences for qRT-PCR are listed in Table 1. The results were calculated using the $2^{-\triangle\triangle Ct}$ method.

Table 1
Primer sequences for qRT-PCR assays.

Primers	Primer Sequences	NCBI Reference Sequence	Product Length (bp)
CAT	CCAGCCCTGACAAAATGCTT AAAGCGGGTCCTATGTTCCA	XM_060400055.1	242
SOD1	GGCAATGTGAAGGCTGACAA TGCCCAAGTCATCTGGTCTT	NM_001145185.2	130
GPX1	CAGTTTGGGCATCAGGAAAAC CGAAGAGCATGAAATTGGGC	XM_004018462.5	100
ATF4	AGGAGGATGCCCACTCAGAT TCTCCAGGAGGGTCGTAAGG	XM_012158819.3	172
DDIT3	GCTGCCCTTCCCTTTTTGACTA CTCAGTAAGCCAAGCCAGAGA	XM_060412904.1	111
BIP	CCGAGACATCACAGACGCTT GTCAGCAGGCAGCTATAGGG	XM_004005637.4	125
GADD34	AGCCGGTGACAACTTGAGTC TGATGGGGTATTTGCCCTGG	XM_012190639.4	178
PERK	GGTGTCATCCAGCCTTAGCA ACAGATGTACCTCACCTTTCCAC	XM_004005901.6	238
ERN1	CAGAAGGATTTCGCCCACCT ACGATGTTGAGGGAGTGCAG	XM_027974337.2	92
ATF6	CTGGGTTCTGGAGGCCGAAG AGCAAACAGGGCAGAATCAGA	XM_042256929.1	70
XBP1	GACCCAGAAGGACCCAGTTC TCACTACCACACTGGCTTCG	XM_004017459.5	169

2.7. Western blotting

Western blotting was conducted to assess the protein expression of catalase (CAT), superoxide dismutase 1 (SOD1), glutathione peroxidase 1 (GPX1), immunoglobulin binding protein (BIP), protein kinase R-like endoplasmic reticulum kinase (PERK), and activating transcription factor 6 (ATF6). Total protein was extracted from cells using RIPA buffer (Solarbio, Beijing, China). The protein samples were heated in a metal bath for 10 min, allowed to cool to room temperature, and then separated by SDS-PAGE. The proteins were transferred onto polyvinylidene difluoride (PVDF) membranes, which were blocked with 5 % skim milk for 2 h. The membranes were incubated overnight at 4 ℃ with primary antibodies against CAT, SOD1, GPX1, ATF6, PERK, BIP (Proteintech, Wuhan, China), and GAPDH (Invitrogen, Carlsbad, CA, USA). Afterward, secondary antibodies were applied, and the membranes were incubated at 37 ℃ for 2 h. Protein bands were visualized using enhanced chemiluminescence, and the results were quantified with ImageJ software.

2.8. RNA-Seq

The selection of NaF working concentration for RNA-Seq refers to our previous study. cDNA library sequencing was performed using an Illumina HiSeqTM 2500/4000 (Gene Denovo Biotechnology Co., Ltd., Guangzhou, China). Bioinformatics analysis was performed using OmicSmart, a real-time interactive online platform for data analysis (http://www.omicsmart.com. Protein–protein interaction (PPI) was constructed by a string online database (https://cn.string-db.org/) and Cytoscape software (version 3.3.0). Fig. 1 shows a flowchart of the experiment.

2.9. Statistical analysis

The data were analyzed using Prism 9.0 software. All values in this study are expressed as mean ± SEM. Statistical analysis of differences among groups was performed using one-way ANOVA or Student's *t*-test. $P < 0.05$ was considered to indicate a significant difference. (*$P < 0.05$; **$P < 0.01$; ***$P < 0.001$; #$P < 0.05$; ##$P < 0.01$; ###$P < 0.001$).

3. Results

3.1. Cell culture and treatment

Fig. 2A shows the microscopic morphology of primary GCs at 0, 24, and 48 h. Freshly isolated GCs were circular and started to grow adherently at 12 h, showing an irregular polygonal or round morphology with clear cell boundaries. All isolated primary and resuscitated cells were free of mycoplasma contamination (Fig. 2B).

3.2. Hoechst 33258 staining

Hoechst 33258 is a nuclear stain, that can penetrate the cell membrane, stain DNA, and emit strong blue fluorescence after embedding double-stranded DNA, which is commonly used for detecting apoptosis. Hoechst 33528 staining reagent was used for the preliminary detection of apoptosis. After staining with Hoechst 33258, nuclei of cells were blue, the control cells had weak nuclear fluorescence, and chromatin was evenly distributed. With increasing NaF concentration, the fluorescence intensity in the experimental groups showed a significant increase, with nuclei showing bright blue fluorescence, dense staining, and condensed appearance, indicating that NaF treatment led to the induction of apoptosis (Fig. 3A). The intensities in the 3.5 and 4 mM NaF-treated groups were notably higher than those in the control group (Fig. 3B). These findings suggest that NaF induces apoptosis in GCs.

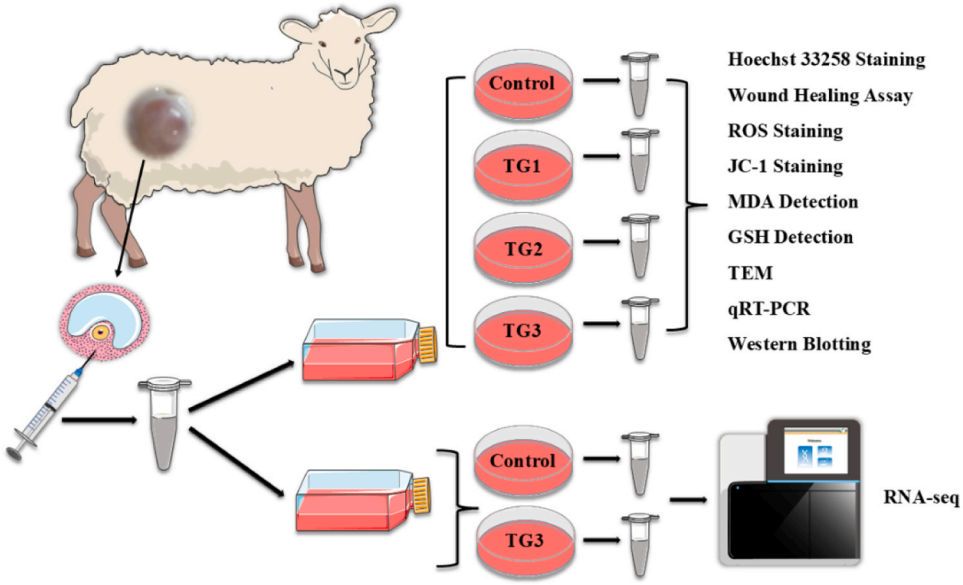

Fig. 1. Flowchart of the experiment.

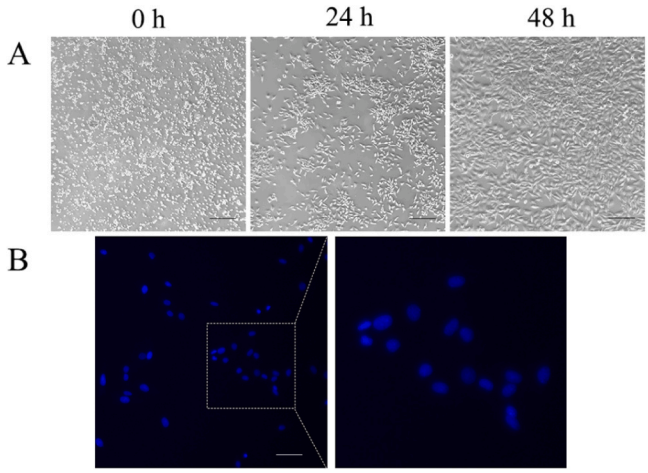

Fig. 2. Cell culture and mycoplasma staining detection. (A) The microscopic morphology of primary GCs at 0, 24, and 48 h (4×, 250 μm). (B) Mycoplasma staining detection (4×, 250 μm).

3.3. Scratch-wound assay

Scratch-wound assay can be used to measure basic cell migration parameters such as speed, persistence, and polarity. In this study, the migration area of the control group exceeded 30 % after 12 h, whereas those of the 3 mM and 3.5 mM NaF-treated groups were < 20 %, and the 4 mM NaF-treated group had the lowest migration area. After 24 h, the migration area of the control group was approximately 60 %, whereas in the NaF-treated groups, the wound area decreased but was not fully closed, indicating a decline in cell migration (Fig. 4A) (Fig. 4B). These findings suggested that NaF reduced the migratory ability of GCs.

3.4. Assessment of ROS, MDA, and GSH levels, and mitochondrial membrane potential

The NaF-treated groups exhibited significant green fluorescence compared to the control group (Fig. 5A). The fluorescence intensities in the 3, 3.5, and 4-mM NaF treatment groups were significantly higher than in the control group, indicating that NaF induced high level of ROS production in GCs to and exacerbated the degree of cellular oxidative stress (Fig. 5C). Additionally, compared to that of the control group, the NaF-treated groups showed enhanced green fluorescence, with a significant increase in JC-1 monomer levels and a notable decrease in mitochondrial membrane potential (Fig. 5B) (Fig. 5D).

MDA levels were significantly increased in the NaF-treated groups, whereas the total GSH levels were significantly reduced compared with the control group (Fig. 5E) (Fig. 5F).

TEM was used to observe changes in the cellular ultrastructure. The results showed that in the control group, cell morphology was relatively normal, with abundant organelles, such as mitochondria and endoplasmic reticulum, and clear and intact structures, with only a few vacuoles. In contrast, NaF-treated cells exhibited irregular morphology with mitochondria showing unclear edges, abnormal shapes, swelling, and vacuolization. The endoplasmic reticulum was mildly expanded, and numerous vacuoles and autophagosomes were present in the cytoplasm (Fig. 5G).

3.5. Fluoride-induced oxidative stress in GCs

qRT-PCR and western blotting were used to measure the expression of oxidative stress-related genes and proteins. The relative mRNA expression levels of *CAT, SOD1*, and *GPX1* in the NaF-treated groups were significantly decreased, compared to that in the control group (Fig. 6A). The protein expression levels of CAT, SOD1, and GPX1 in the NaF-treated groups were significantly decreased, compared to that in the control group (Fig. 6B). When GCs were cotreated with N-acetylcysteine (NAC) and NaF, CAT, SOD1, and GPX1 expression was significantly increased in the NAC-treated group (Fig. 6C). Additionally, ROS levels in the NAC-treated group were significantly lower than those in the NaF-treated group. The NAC+NaF-treated group showed significantly less ROS production than the NaF-treated group, indicating that NAC reduced ROS levels and alleviated NaF-induced oxidative stress in GCs (Fig. 6D).

3.6. Fluoride-induced ERS in GCs

The expression of ERS-related genes and proteins were analyzed by qRT-PCR and western blotting. The mRNA levels of *BIP, PERK, ATF4, ATF6, CHOP, GADD34, ERN1*, and *XBP1* were significantly increased in the NaF-treated groups compared to that in the control group (Fig. 7A).

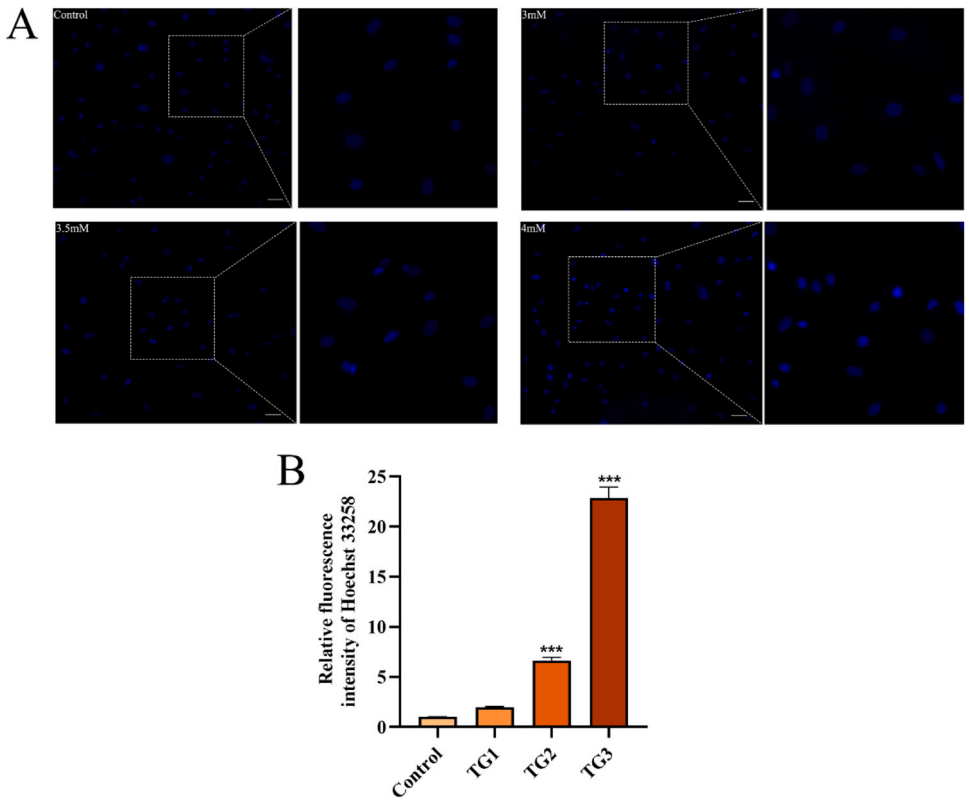

Fig. 3. Hoechst 33258 Staining. (A) Hoechst 33258 Staining of GCs in the 3, 3.5, and 4-mM NaF treatment groups (4×, 250 μm). (B) Fluorescence intensity of Hoechst 33258 staining. *** $p < 0.001$.

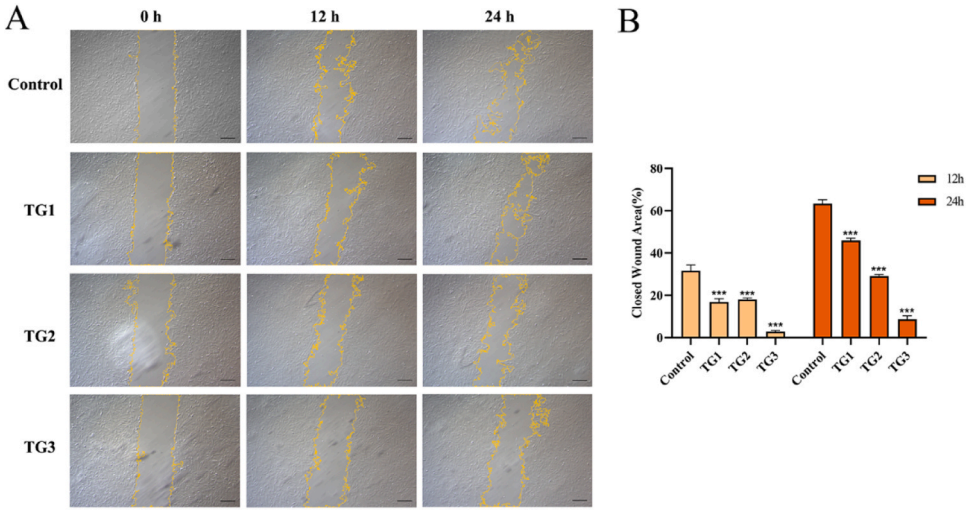

Fig. 4. Scratch-Wound Assay. (A) Scratch-Wound Assay of GCs in the 3, 3.5, and 4-mM NaF treatment groups (4×, 250 μm). (B) Histogram of GCs closed wound area (%) at 12 and 24 h. *** $p < 0.001$.

Moreover, BIP, PERK, and ATF6 levels were significantly increased in the NaF-treated group compared to those in the control group, indicating that fluoride induced ERS in GCs (Fig. 7B). Treatment of cells with the ERS inhibitor GSK2656157 significantly reduced the ERS induced by NaF in GCs. Compared to that in the NaF-treated group, the mRNA expression of *BIP, PERK, ATF4, ATF6, CHOP, GADD34, ERN1*, and *XBP1* were significantly decreased in the NaF + GSK2656157-treated group (Fig. 7C), and BIP, PERK, and ATF6 levels were significantly reduced (Fig. 7D). Finally, we used the Mitochondrial Membrane Potential Assay Kit to assess the mitochondrial membrane potential levels in the cells. The results indicated that, compared to the NaF-treated group, NaF + GSK2656157 treatment restored the mitochondrial membrane potential decreased by NaF treatment (Fig. 7E) (Fig. 7F).

3.7. Analysis of RNA-Seq data

The correlation coefficients between samples were calculated based on the fragments per kilobase of transcript per million mapped reads (FPKM)/transcripts per million (TPM) values, and the repeatability of samples within groups was assessed. The FPKM/TPM values were log-

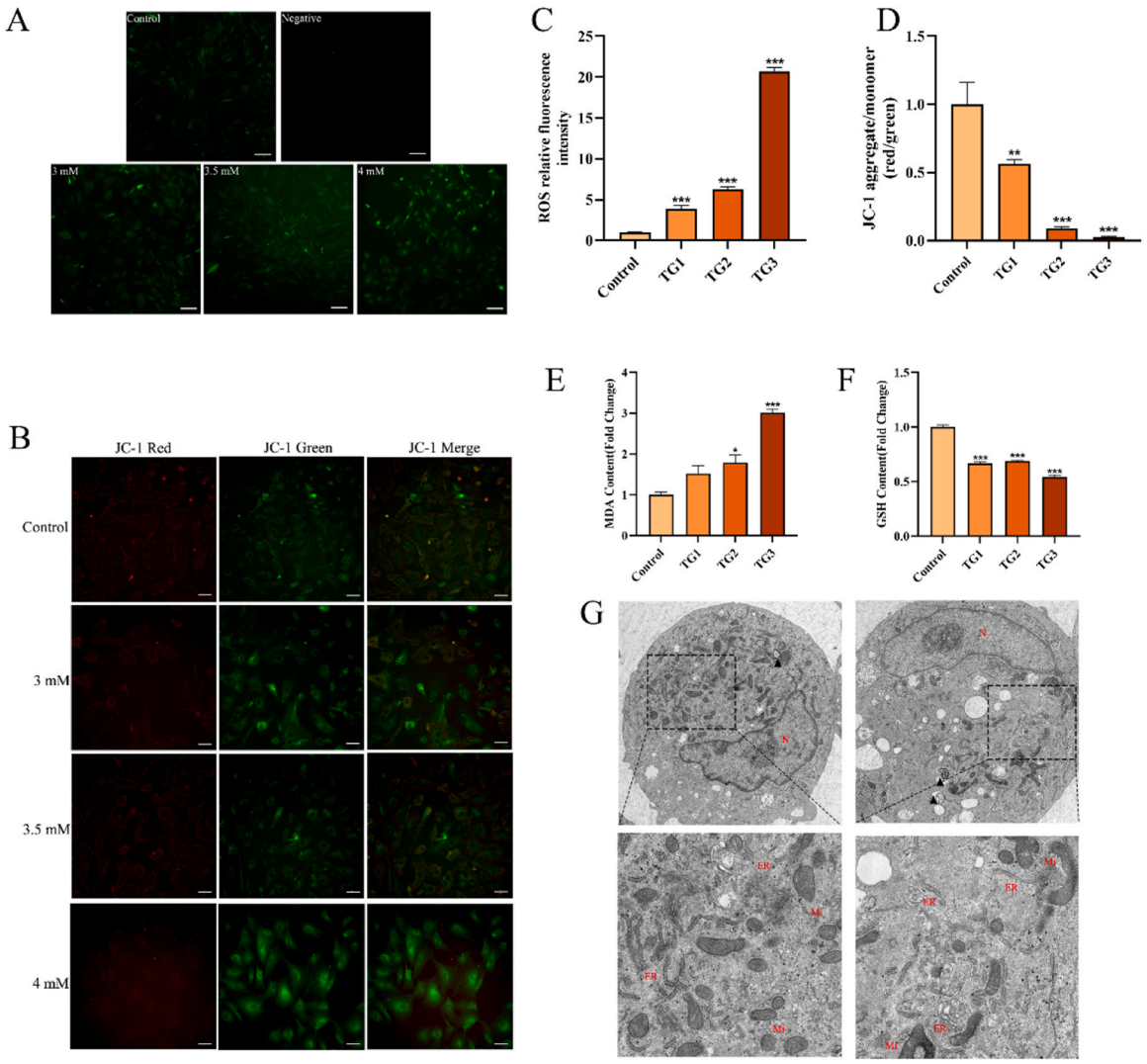

Fig. 5. Assessment of Reactive Oxygen Species (ROS), MDA, and Reduced Glutathione (GSH) Levels, and Mitochondrial Membrane Potential (MMP). (A) ROS staining results of GCs in the 3, 3.5, and 4-mM NaF treatment groups (10 ×, 100 μm) Negative control: cells only (no working solution) (B) MMP staining results of GCs in the 3, 3.5, and 4-mM NaF treatment groups (20 ×, 50 μm). (C) ROS relative fluorescence intensity. *** $p < 0.001$. (D) MMP fluorescence intensity. (E-F) MDA and GSH content of GCs in the 3, 3.5, and 4-mM NaF treatment groups. *** $p < 0.001$. (G) Representative TEM images of GCs in the control and 4-mM NaF treatment groups.

transformed (log_{10}) prior to plotting. As shown in Fig. 8A, the Pearson correlation coefficients between samples of the control and treated groups were both > 0.999, indicating a good correlation. In the scatter plot and fitted line, most of the data points were located along the diagonal, indicating considerable repeatability among the samples. Principal component analysis (PCA) was performed based on gene expression data to compare samples within and between groups. Samples from the control group and NaF-treated group showed distinct clusters (Fig. 8B). The transcript of the differentially expressed genes (DEGs) was mapped to the Gene Ontology (GO) database, including the GO terms molecular function (MF), cellular component (CC), and biological process (BP). DEGs were enriched and categorized, and a bubble plot was generated to show the 20 top enriched GO terms (Fig. 8C). We summarized the DEGs related to oxidative stress and ERS, and generated a heat map (Fig. 9A) (Fig. 9B). The heatmap showed results consistent with those of previous studies. Additionally, a protein–protein interaction (PPI) network diagram was constructed using String and visualized in Cytoscape (Fig. 9C). The PPI network comprised 17 nodes, including eight ERS proteins, ERN1, ATF6, ATF4, PPP1R15A, DDIT3, XBP1, EIF2AK3, HSPA5 and nine oxidative stress proteins, GPX2, GPX3, GPX5, GPX7, GPX8, SOD1, SOD3, CAT and HMOX1.

4. Discussion

With rapid economic development, toxic substances are being continuously released into the environment. These substances enter the body directly or indirectly through the atmosphere, water, soil, and food, leading to disorders of the endocrine system and posing a threat to human and animal health. One such compound is fluoride (Solanki et al., 2022). Adequate fluoride intake helps prevent osteoporosis and dental caries, however, prolonged exposure to fluoride can lead to fluoride poisoning, causing severe damage to the body. Fluoride poisoning is prevalent in several countries, with more than 200 million people currently affected by fluorosis (Wu et al., 2022b). Over 80 % of rural villages in Africa and Asia have excessive fluoride concentrations in the groundwater, and more than 100 million people are affected by skeletal fluorosis (Srivastava and Flora, 2020). Exposure to high fluoride concentrations in drinking water is associated with a decrease in birth rate (Freni, 1994). Long-term exposure to fluoride has been linked to menstrual abnormalities in female workers, increased frequency of miscarriages, and pregnancy complications (Zhang et al., 2007).

The ovary is a crucial component of the female reproductive system and structural changes can significantly impact female reproductive

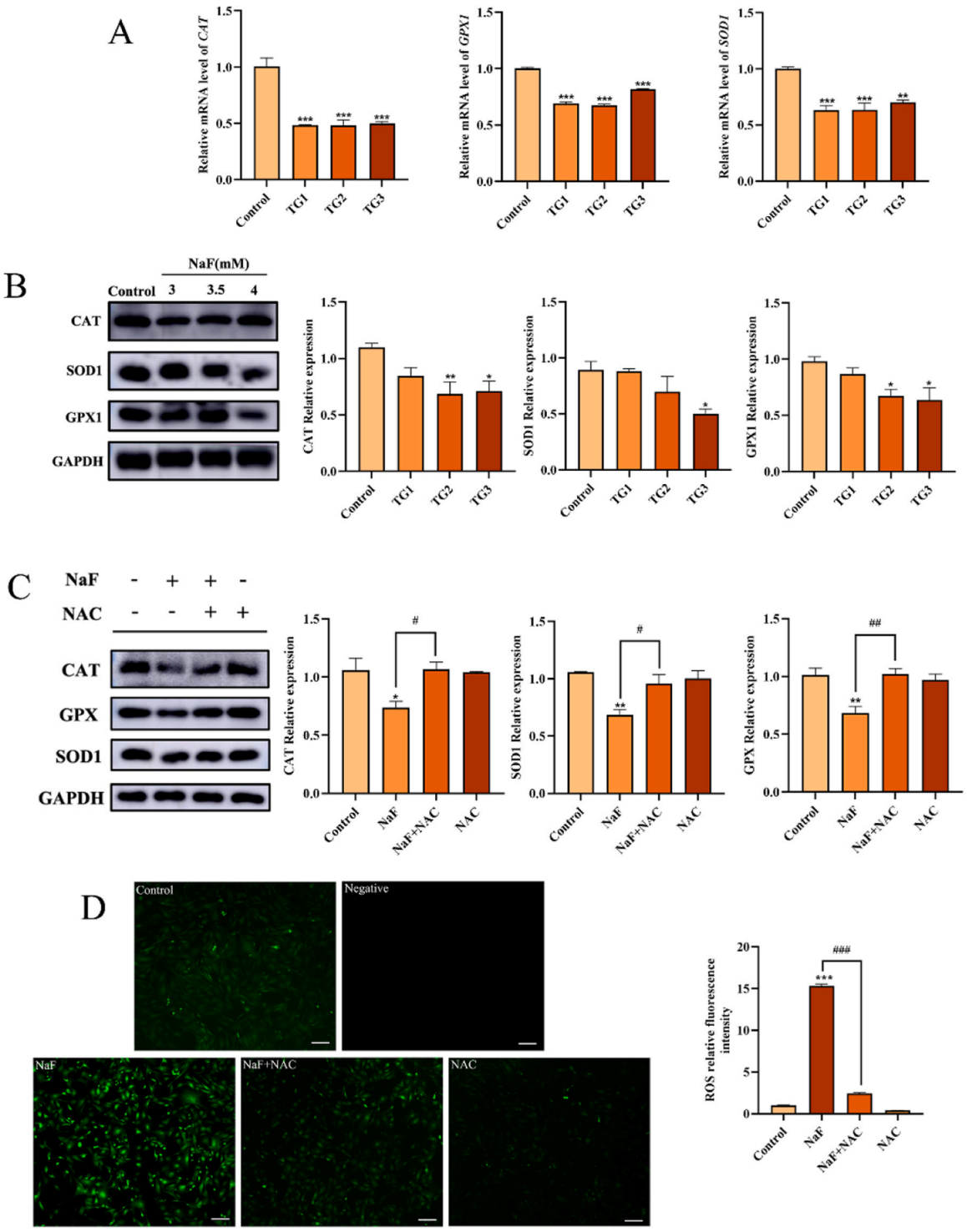

Fig. 6. Fluoride-induced oxidative stress in GCs. (A) Relative mRNA expression levels of *CAT*, *GPX1*, and *SOD1*. (B) The protein expression levels of CAT, GPX1, and SOD1. (C) The protein expression levels of CAT, GPX1, and SOD1 after treatment with NAC. (D) ROS staining results of GCs treated with NaF (4 mM) and NAC (45 μM) (10×, 100 μm). Negative control: cells only (no working solution) * $p < 0.05$, ** $p < 0.01$, *** $p < 0.001$, # $p < 0.05$, ## $p < 0.01$, ###$p < 0.001$.

function. Fluoride intake leads to damage to ovarian and uterine tissues, reduced ovarian weight (Al-Hiyasat et al., 2000), enlargement of endometrial cells, hypertrophy of endometrial glands, suppression of oocyte and GC growth, abnormal secretion of reproductive hormones (E2, FSH, LH, GnRH, P4 and T), inhibition of mature follicle development, and ultimately disruption of the reproductive system, leading to female infertility (Al-Okaily and Ali, 2019; Chaithra et al., 2019; Fishta et al., 2024; Pushpalatha et al., 2005; Zhou et al., 2013a; Zhou et al., 2013b). Therefore, fluoride directly affects follicular differentiation and maturation, ultimately impairing the reproductive system.

Oxidative stress, which is involved in various physiological and pathological processes, refers to an abnormal state resulting from an imbalance between ROS production and the antioxidant systems of the body, leading to cellular damage (Li et al., 2023). Oxidative stress has also been recognized as a mechanism underlying fluoride toxicity. When an organism is exposed to harmful fluoride stimuli, an imbalance

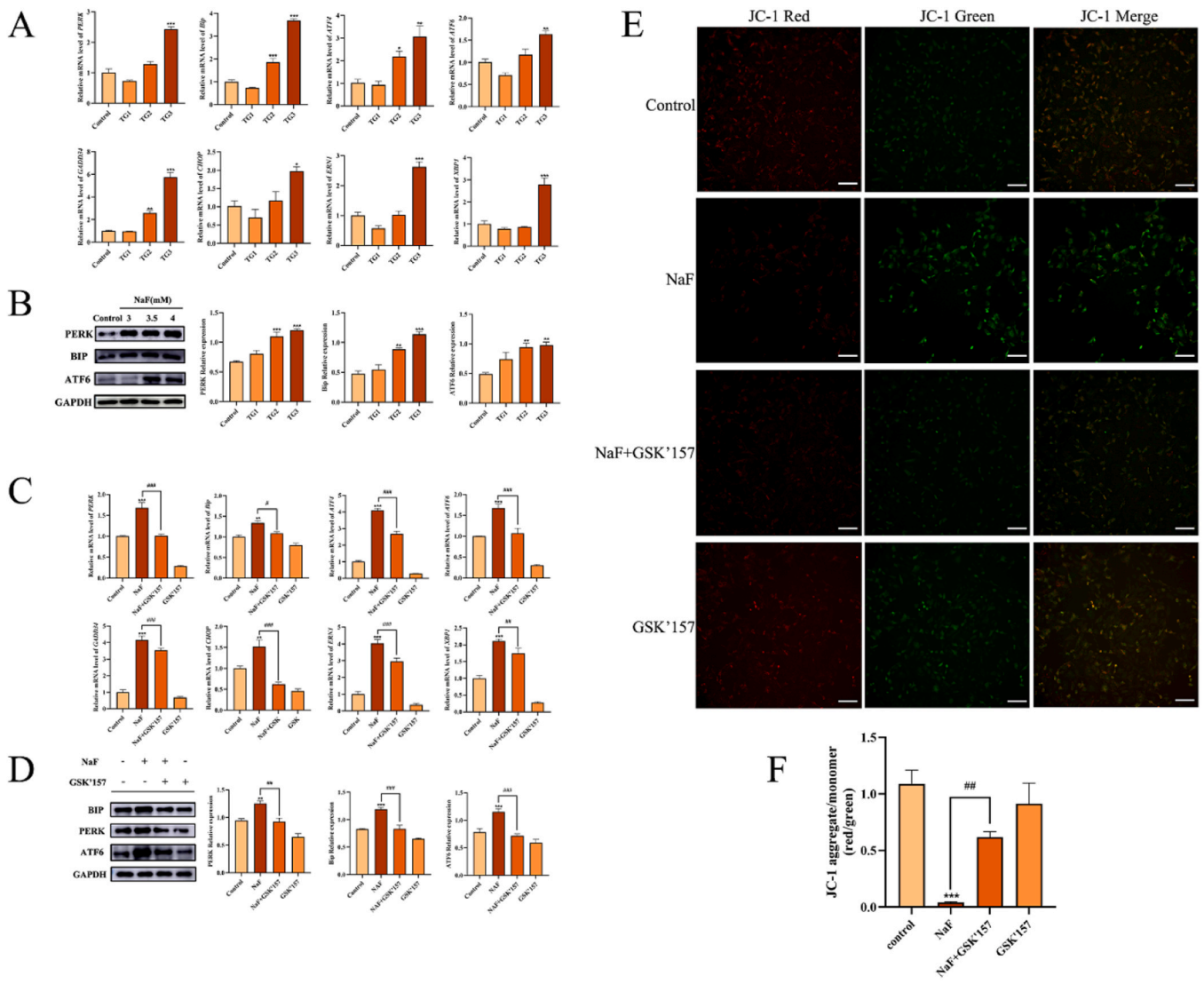

Fig. 7. Fluoride-induced ERS in GCs. (A) Relative mRNA expression levels of *BIP, PERK, ATF4, ATF6, CHOP, GADD34, ERN1*, and *XBP1*. (B) The protein expression levels of PERK, BIP, and ATF6. (C) Relative mRNA expression levels of *BIP, PERK, ATF4, ATF6, CHOP, GADD34, ERN1*, and *XBP1* after treatment with GSK2656157. (D) The protein expression levels of PERK, BIP, and ATF6 after treatment with GSK2656157. (E-F) MMP staining results of GCs in different treatment groups (4×, 250 μm). * $p < 0.05$, ** $p < 0.01$, *** $p < 0.001$, # $p < 0.05$, ## $p < 0.01$, ###$p < 0.001$.

between oxidation and anti-oxidation leads to lipid peroxide production, causing oxidative stress. SOD and CAT are the crucial antioxidant enzymes, which remove free radicals. Inhibition of their activity inevitably damages the body. SOD combines with GSH to convert superoxide free radicals into hydrogen peroxide and water, protecting cells from damage to biomolecules such as DNA caused by ROS. (Cao et al., 2013). MDA is the end product of lipid peroxidation. Disruption of the balance between oxidation and antioxidation leads to abnormal MDA levels, indicating oxidative stress and cellular damage. At certain stages of fluoride poisoning, increases in free radical formation and induction of oxidative stress occur. F-poisoning owing to high fluoride exposure induces oxidative stress in humans and animals. In regions with endemic fluorosis, the total antioxidant capacity in the plasma of affected populations is significantly reduced, and the oxidative stress index of the body is notably elevated (Varol et al., 2011). This highlights the role of oxidative stress in fluoride toxicity and its potential to cause cell and tissue damage. Fluoride poisoning significantly decreases the levels of CAT, GSH, and SOD, in brain tissue of rats, while H_2O_2 and MDA levels significantly increase, leading to enhanced oxidative stress (Ma et al., 2023; Tian et al., 2019). Other organs, such as the liver, kidneys, testes, ovary and uterus, also experience varying degrees of damage (Fishta et al., 2024; Ray et al., 2020; Samir, 2017; Song et al., 2020; Sun et al., 2017; Zhang et al., 2014). Moreover, excessive fluoride intake disrupts the metabolism of trace elements in the body, which, in turn, affects the synthesis of various antioxidant enzymes, resulting in a significant increase in intracellular free radicals and causing cell and tissue damage (Fishta et al., 2024; Podder et al., 2015; Rana et al., 2024; Zhong et al., 2020). According to a review, fluoride exposure exerts significant adverse effects on the reproductive system by disrupting antioxidant homeostasis, leading to sperm damage and oocyte abnormalities, ultimately compromising fertility (Talebi et al., 2025). Our experimental results showed that fluoride exposure significantly reduced the mRNA and protein levels of CAT, SOD1, and GPX1 in GCs. The changes in MDA and GSH levels were consistent with previous findings. This provides additional validation for our initial hypothesis concerning fluoride-induced ovine GCs damage mechanisms. Fluoride exposure can inhibit or deplete the activity of antioxidant enzymes in the body, thereby causing oxidative stress in ovine GCs. Excessive production of ROS and lipid peroxides disrupts the balance between the oxidative and antioxidative systems in GCs, ultimately causing cellular damage. NAC

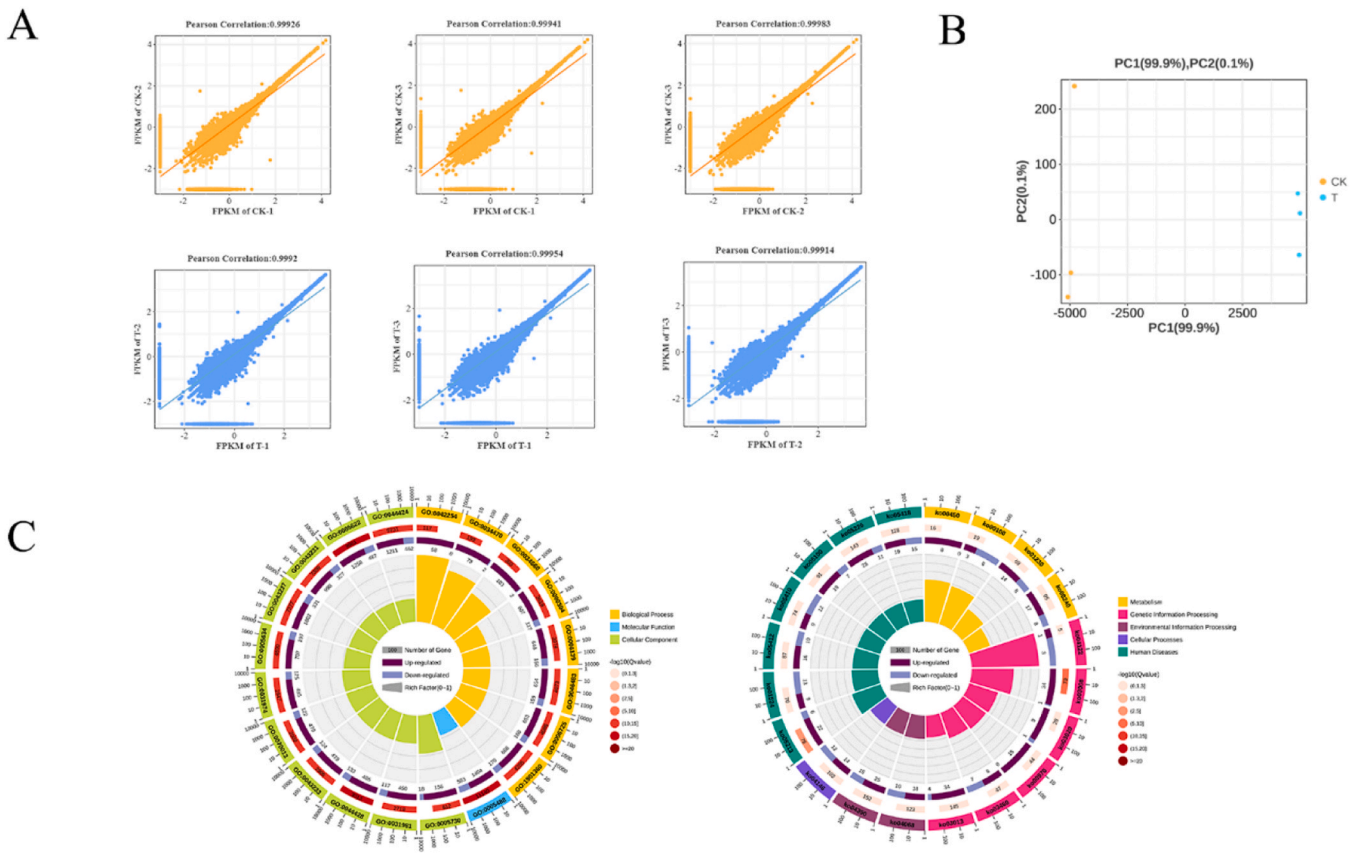

Fig. 8. Analysis of RNA-Seq Data. (A) Sample Relationship Repeatability Scatter Chart. (B) The PCA plot. (C) GO and KEGG enrichment circle diagram.

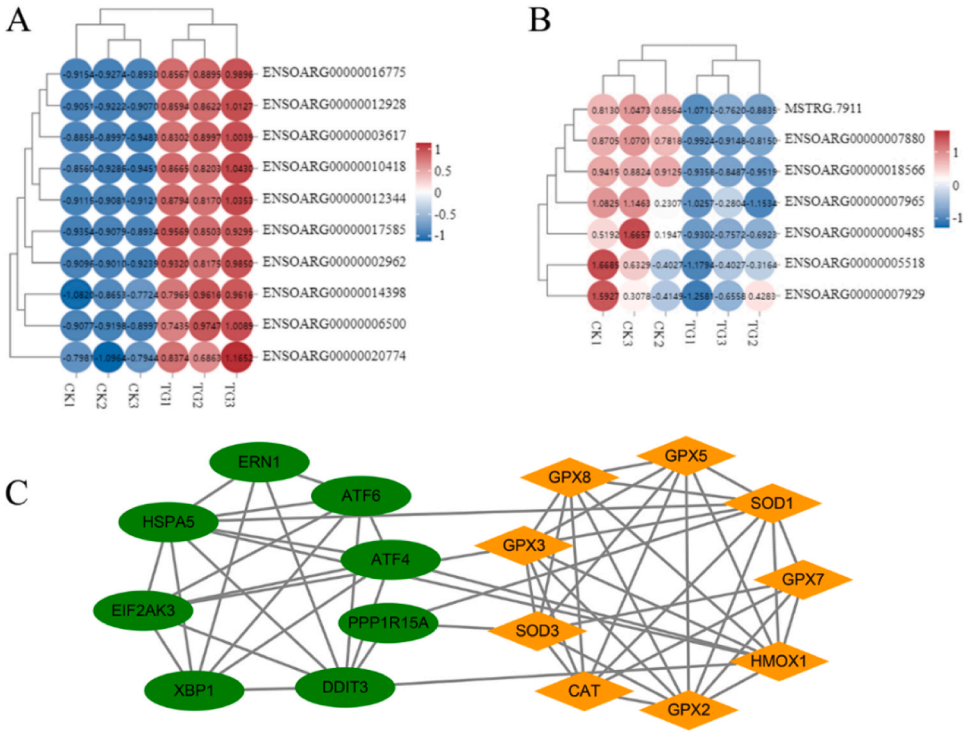

Fig. 9. Results of DEG classification analysis of RNA-Seq. (A) Heat map of the DEGs related to oxidative stress. (B) Heat map of the DEGs related to ERS. (C) PPI network diagram of genes.

is a commonly used antioxidant, which primarily scavenges free radicals and peroxides by providing sulfhydryl groups (-SH), thereby inhibiting ROS generation and accumulation (Pedre et al., 2021). Our results indicated that NAC combined with NaF treatment significantly reduced ROS levels in cells. Furthermore, NAC intervention effectively restored the NaF-induced reduction of CAT, SOD1, and GPX1 expression. Therefore, our findings confirm that NAC alleviates NaF-induced damage in GCs by suppressing oxidative stress.

In addition to causing excessive production of H_2O_2, MDA, and NO, fluoride can lead to the accumulation of misfolded proteins in the endoplasmic reticulum, resulting in ERS and ROS generation (Barbier et al., 2010; Hassan and Yousef, 2009). The endoplasmic reticulum is a crucial organelle, which plays an essential role in maintaining cellular stability (Govindarajan et al., 2020). It is responsible for the synthesis, folding, and maturation of proteins within cells (Duwaerts and Maiers, 2022; Feng and Anderson, 2017). Owing to external stimuli, the disruption of endoplasmic reticulum homeostasis leads to ERS. In the short term, ERS serves as an adaptive response to enhance the cell's ability to handle unfolded or misfolded proteins, restoring endoplasmic reticulum homeostasis, and promoting cell survival. However, if the adaptive capacity of unfolded protein response is exceeded, cell death may occur (Lebeau et al., 2022; Ren et al., 2021). Oxidative stress and ERS interact with each other, and oxidative stress can exacerbate ERS by disturbing protein folding and increasing the load of misfolded proteins. In contrast, ERS amplifies oxidative stress through ROS generation. This vicious cycle can lead to significant cellular dysfunction and apoptosis, specifically in sensitive cell types such as granulosa cells. Fluoride exposure induces an increase in GRP78 level in the cortical regions of rats (Wei et al., 2025). Fluoride treatment significantly increases the expression of ATF4, C/EBP homologous protein (CHOP), and GRP78 in jejunal epithelial cells of chicks (Li et al., 2024). Fluoride exposure causes heart tissue damage and expansion of the endoplasmic reticulum in chickens, with increased expression of PERK, ATF4, CHOP, IRE1, EIF2α, and ATF6 (Hou et al., 2024). Excessive fluoride induces the apoptosis of enamel cells by activating ERS, which is mediated by the GRP-78/PERK/CHOP signaling pathway (Jinyi et al., 2023). NaF treatment induces ERS in Sertoli cells, manifested as the upregulation of GRP78, PERK, and CHOP expression (Yang et al., 2015). Our results indicated that fluoride exposure significantly upregulated the mRNA expression of ERS-related genes *BIP, PERK, ATF4, ATF6, CHOP, GADD34, ERN1*, and *XBP1* in GCs and BIP, PERK, and ATF6 levels, suggesting that fluoride can induce ERS in GCs. Furthermore, the ERS inhibitor GSK2656157 significantly reduced NaF-induced elevation of gene and protein expression and restored the mitochondrial membrane potential. These findings are consistent with those of previous studies demonstrating that fluoride can induce oxidative stress and ERS in GCs. Finally, we inferred a conceptual diagram of fluoride-induced oxidative stress and ERS in GCs (Fig. 10).

This study has a limitation. Due to sampling limitations, the effect of fluoride on ovine oocytes was not evaluated in this study. Because of the high economic cost and complexity involved in animal studies, and numerous uncontrollable factors, we only conducted experiments using primary ovine cells and did not conduct *in vivo* experiments. Future studies incorporating in vitro maturation of oocytes may provide a more comprehensive understanding of fluoride-induced reproductive toxicity in female ovine. We also plan to conduct related research using animal models, and intend to screen for potential drugs that can mitigate fluoride toxicity in both cellular and animal models, with the aim of providing more data and theoretical support for future studies.

5. Conclusion

Taken together, our results demonstrate that exposure to different concentrations of NaF in GCs induced oxidative stress, leading to increased levels of ROS and MDA, and a decrease in GSH, along with an elevation in mitochondrial membrane potential. Fluoride inhibited cell migration and induced ultrastructural alterations, featuring mitochondrial swelling with vacuolization, endoplasmic reticulum dilation, and cytoplasmic accumulation of autophagic vacuoles. Simultaneously, ERS was activated, with upregulation of oxidative stress and ERS-related genes and proteins. NAC can effectively inhibit the accumulation of ROS, while GSK2656157 can significantly reduce the expression of ERS-related genes and proteins. This study contributes to a deep understanding of fluoride-induced toxicity of the female reproductive system and provides a foundation for mitigating its impact on the reproductive health of animals and humans.

CRediT authorship contribution statement

Wanruo Liu: Investigation. **Didi Jiang:** Resources, Investigation. **Kun Gao:** Investigation. **Zongshuai Li:** Visualization. **Tian Ma:** Writing – original draft, Visualization, Validation, Software, Resources, Methodology, Investigation, Formal analysis, Data curation, Conceptualization. **Yong Zhang:** Writing – review & editing, Supervision, Project administration, Funding acquisition.

Funding

This research was funded by the Gansu Key Laboratory of Animal Generational Physiology and Reproductive Regulation (20JR10RA563) and the 13th Five-Year National Key Research and Development Plan Food Safety Technology Research and Development Major Project (2019YFC1605705).

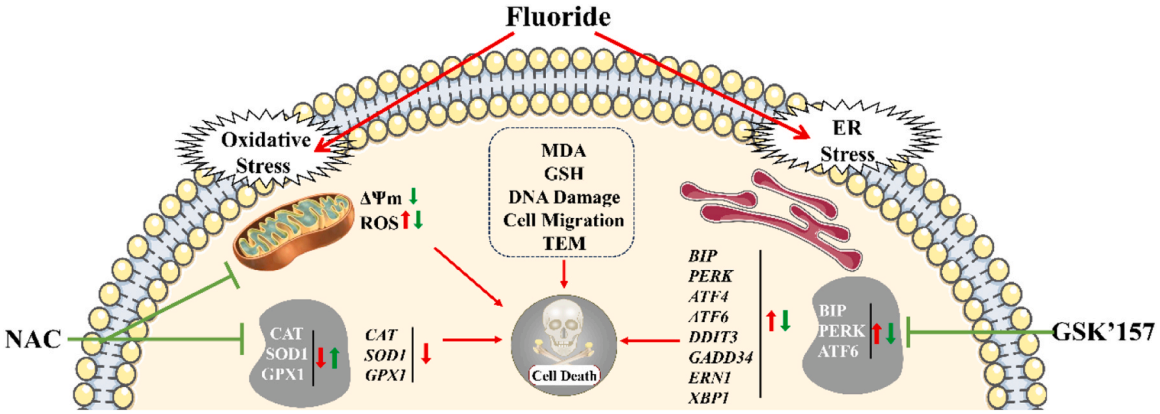

Fig. 10. Conceptual diagram of the regulation of fluoride-induced oxidative stress and ERS in GCs.

Declaration of Competing Interest

The authors declare that they have no known competing financial interests or personal relationships that could have appeared to influence the work reported in this paper.

Acknowledgements

We are grateful for the help and understanding of the Gansu Key Laboratory of Animal Generational Physiology and Reproductive Regulation.

Data availability

The data that support the findings of this study are available from the corresponding author upon reasonable request.

References

Al-Hiyasat, Ahmad S., Elbetieha, Ahmed M., Darmani, Homa, Irbid, Jordan, 2000. Reproductive toxic effects of ingestion of sodium fluoride in female rats.
Al-Okaily, Baraa Najim, Ali, Ellaf Hussian, 2019. Effect of pomegranate seed oil against Hepatotoxicity- induced by sodium. Iraqi J. Vet. Med.
Barbier, O., et al., 2010. Molecular mechanisms of fluoride toxicity. Chem. Biol. Interact. 188, 319–333.
Cao, J., et al., 2013. Effects of fluoride on liver apoptosis and Bcl-2, bax protein expression in freshwater teleost, cyprinus carpio. Chemosphere 91, 1203–1212.
Cavalcanti, G.S., et al., 2023. Granulosa cells and follicular development: a brief review. Revista da Associação Médica Brasileira 69.
Chaithra, B., et al., 2019. A comparative analysis of fluoride-contaminated groundwater and sodium fluoride-induced reproductive toxicity and its reversibility in male rats. Biol. Trace Elem. Res. 197, 507–521.
Chen, Q., et al., 2021. miR-378d is involved in the regulation of apoptosis and autophagy of and E2 secretion from cultured ovarian granular cells treated by sodium fluoride. Biol. Trace Elem. Res. 199, 4119–4128.
Choubisa, S.L., Choubisa, D., 2016. Status of industrial fluoride pollution and its diverse adverse health effects in man and domestic animals in India. Environ. Sci. Pollut. Res. 23, 7244–7254.
Cortinovis, C., et al., 2014. Effects of fumonisin B1 alone and combined with deoxynivalenol or zearalenone on porcine granulosa cell proliferation and steroid production. Theriogenology 81, 1042–1049.
Duwaerts, C.C., Maiers, J.L., 2022. ER disposal pathways in chronic liver disease: protective, pathogenic, and potential therapeutic targets. Front. Mol. Biosci. 8.
Efe, U., et al., 2020. Apoptotic and oxidative mechanisms in liver and kidney tissues of sheep with fluorosis. Biol. Trace Elem. Res. 199, 136–141.
Feng, N., Anderson, M.E., 2017. CaMKII is a nodal signal for multiple programmed cell death pathways in heart. J. Mol. Cell. Cardiol. 103, 102–109.
Fishta, A., et al., 2024. Effects of fluoride toxicity on female reproductive system of mammals: a meta-analysis. Biol. Trace Elem. Res. 203, 646–669.
Freni, S.C., 1994. Exposure to high fluoride concentrations in drinking water is associated with decreased birth rates. J. Toxicol. Environ. Health 42, 109–121.
Geng, N., et al., 2024. Excessive fluoride induces ovarian function impairment by regulating levels of ferroptosis in fluorosis women and ovarian granulosa cells. Reprod. Toxicol. 125.
Govindarajan, S., et al., 2020. ER stress in antigen-presenting cells promotes NKT cell activation through endogenous neutral lipids. EMBO Rep. 21.
Hassan, H.A., Yousef, M.I., 2009. Mitigating effects of antioxidant properties of black berry juice on sodium fluoride induced hepatotoxicity and oxidative stress in rats. Food Chem. Toxicol. 47, 2332–2337.
Hou, L., et al., 2024. A new insight into fluoride induces cardiotoxicity in chickens: involving the regulation of PERK/IRE1/ATF6 pathway and heat shock proteins. Toxicology 501.
Jinyi, L., et al., 2023. ERS mediated by GRP-78/PERK/CHOP signaling is involved in fluoride-induced ameloblast apoptosis. Biol. Trace Elem. Res. 202, 1103–1114.
Laurindo, L.F., et al., 2024. Mechanisms and effects of AdipoRon, an adiponectin receptor agonist, on ovarian granulosa cells—a systematic review. Naunyn-Schmiedeberg's Arch. Pharmacol. 398, 1305–1314.
Lebeau, G., et al., 2022. Evidence of RedOX imbalance during zika virus infection promoting the formation of disulfide-bond-dependent oligomers of the envelope protein. Viruses 14.
Li, J., et al., 2023. Recent progress of oxidative stress associated biomarker detection. Chem. Commun. 59, 7361–7374.
Li, Y., et al., 2021. The potential risks of chronic fluoride exposure on nephrotoxic via altering glucolipid metabolism and activating autophagy and apoptosis in ducks. Toxicology 461.
Li, Y., et al., 2024. Fluoride stimulates the MAPK pathway to regulate endoplasmic reticulum stress and heat shock proteins to induce duodenal toxicity in chickens. Poult. Sci. 103.
Liang, C., et al., 2020. Fluoride induced mitochondrial impairment and PINK1-mediated mitophagy in leydig cells of mice: in vivo and in vitro studies. Environ. Pollut. 256.
Liang, S., et al., 2017. Sodium fluoride exposure exerts toxic effects on porcine oocyte maturation. Sci. Rep. 7.
Liu, L., et al., 2023. Effects of zearalenone on apoptosis and copper accumulation of goat granulosa cells in vitro. Biology 12.
Ma, T., et al., 2024. Analysis of toxic effects of fluoride on ovine follicular granulosa cells using RNA-Seq. Antioxidants 13.
Ma, Y.-L., et al., 2023. Enhanced expression of RAGE/NADPH oxidase signaling pathway and increased level of oxidative stress in brains of rats with chronic fluorosis and the protective effects of blockers. J. Trace Elem. Med. Biol. 80.
Öncü, M., et al., 2007. Effect of Long-term fluoride exposure on lipid peroxidation and histology of testes in First- and Second-generation rats. Biol. Trace Elem. Res. 118, 260–268.
Ottappilakkil, H., et al., 2022. Fluoride induced neurobehavioral impairments in experimental animals: a brief review. Biol. Trace Elem. Res. 201, 1214–1236.
Pedre, B., et al., 2021. The mechanism of action of N-acetylcysteine (NAC): the emerging role of H2S and sulfane sulfur species. Pharmacol. Ther. 228.
Pizzo, F., et al., 2016. In vitro effects of deoxynivalenol and zearalenone major metabolites alone and combined, on cell proliferation, steroid production and gene expression in bovine small-follicle granulosa cells. Toxicon 109, 70–83.
Podder, S., et al., 2015. Interaction of DNA-lesions induced by sodium fluoride and radiation and its influence in apoptotic induction in cancer cell lines. Toxicol. Rep. 2, 461–471.
Pramanik, S., Saha, D., 2017. The genetic influence in fluorosis. Environ. Toxicol. Pharmacol. 56, 157–162.
Pushpalatha, T., et al., 2005. Exposure to high fluoride concentration in drinking water will affect spermatogenesis and steroidogenesis in Male albino rats. BioMetals 18, 207–212.
Rahim, A., et al., 2022. A comprehensive review on endemic and experimental fluorosis in sheep: its diverse effects and prevention. Toxicology 465.
Rana, S., et al., 2024. Fluoride-Induced alterations in the pancreas of mammals: a Meta-analysis. Biol. Trace Elem. Res.
Ray, D., et al., 2020. The leaf extracts of camellia sinensis (Green tea) ameliorate sodium fluoride-induced oxidative stress and testicular dysfunction in rats. Asian Pac. J. Reprod. 9.
Ren, H., et al., 2021. The Cross-Links of endoplasmic reticulum stress, autophagy, and neurodegeneration in Parkinson's disease. Front. Aging Neurosci. 13.
Richards, J.S., Pangas, S.A., 2010. The ovary: basic biology and clinical implications. J. Clin. Investig. 120, 963–972.
Samir, D., 2017. Study of Fluoride-Induced haematological alterations and liver oxidative stress in rats. World J. Pharm. Pharm. Sci. 211–221.
Solanki, Y.S., et al., 2022. Fluoride occurrences, health problems, detection, and remediation methods for drinking water: a comprehensive review. Sci. Total Environ. 807.
Song, C., et al., 2020. AMPK/p38/Nrf2 activation as a protective feedback to restrain oxidative stress and inflammation in microglia stimulated with sodium fluoride. Chemosphere 244.
Spicer, L.J., et al., 2025. Granulosa cell function in domestic animals: a review on the in vitro effects of FSH, insulin and insulin-like growth factor 1. Domest. Anim. Endocrinol. 91.
Srivastava, S., Flora, S.J.S., 2020. Fluoride in drinking water and skeletal fluorosis: a review of the global impact. Curr. Environ. Health Rep. 7, 140–146.
Sun, Z., et al., 2016. Fluoride decreased the sperm ATP of mice through inhabiting mitochondrial respiration. Chemosphere 144, 1012–1017.
Sun, Z., et al., 2017. Effects of fluoride on SOD and CAT in testis and epididymis of mice. Biol. Trace Elem. Res. 184, 148–153.
Suzuki, M., et al., 2015. Fluoride induces oxidative damage and SIRT1/autophagy through ROS-mediated JNK signaling. Free Radic. Biol. Med. 89, 369–378.
Talebi, S.F., et al., 2025. Fluoride-induced testicular and ovarian toxicity: evidence from animal studies. Biol. Res. 58.
Tian, X., et al., 2019. Subchronic exposure to arsenite and fluoride from gestation to puberty induces oxidative stress and disrupts ultrastructure in the kidneys of rat offspring. Sci. Total Environ. 686, 1229–1237.
Varol, E., et al., 2011. Evaluation of total oxidative status and total antioxidant capacity in patients with endemic fluorosis. Toxicol. Ind. Health 29, 175–180.
Vasisth, D., et al., 2024. Fluoride and its implications on oral health: a review. J. Pharm. Bioallied Sci. 16, S49–S52.
Wang, D., et al., 2023. Novel pathways of fluoride-induced hepatotoxicity: P53-dependent ferroptosis induced by the SIRT1/FOXOs pathway and Nrf2/HO-1 pathway. Comp. Biochem. Physiol. Part C Toxicol. Pharmacol. 264.
Wang, H.-w, et al., 2017. The MMP-9/TIMP-1 system is involved in Fluoride-Induced reproductive dysfunctions in female mice. Biol. Trace Elem. Res. 178, 253–260.
Wei, D., et al., 2025. Protective effects of anthocyanins on the nervous system injury caused by fluoride-induced endoplasmic reticulum stress in rats. Food Chem. Toxicol. 200.
Wu, H., et al., 2022a. Folic acid ameliorates the declining quality of sodium fluoride-exposed mouse oocytes through the Sirt1/Sod2 pathway. Aging Dis. 13.
Wu, S., et al., 2022b. Challenges of fluoride pollution in environment: mechanisms and pathological significance of toxicity – a review. Environ. Pollut. 304.
Yang, Y., et al., 2015. Sodium fluoride induces apoptosis through reactive oxygen species-mediated endoplasmic reticulum stress pathway in sertoli cells. J. Environ. Sci. 30, 81–89.
Zhang, M., et al., 2007. Effects of fluoride on the expression of NCAM, oxidative stress, and apoptosis in primary cultured hippocampal neurons. Toxicology 236, 208–216.
Zhang, S., et al., 2013. Fluoride-elicited developmental testicular toxicity in rats: roles of endoplasmic reticulum stress and inflammatory response. Toxicol. Appl. Pharmacol. 271, 206–215.

Zhang, Z., et al., 2014. Maize purple plant pigment protects against fluoride-induced oxidative damage of liver and kidney in rats. Int. J. Environ. Res. Public Health 11, 1020–1033.
Zhao, W.-p, et al., 2019. Mitochondrial respiratory chain complex abnormal expressions and fusion disorder are involved in fluoride-induced mitochondrial dysfunction in ovarian granulosa cells. Chemosphere 215, 619–625.
Zhao, W.-P., et al., 2018. JNK/STAT signalling pathway is involved in fluoride-induced follicular developmental dysplasia in female mice. Chemosphere 209, 88–95.
Zhong, N., et al., 2020. Effects of fluoride on oxidative stress markers of lipid, gene, and protein in rats. Biol. Trace Elem. Res. 199, 2238–2246.
Zhou, Y., et al., 2013a. The toxicity mechanism of sodium fluoride on fertility in female rats. Food Chem. Toxicol. 62, 566–572.
Zhou, Y., et al., 2013b. Effects of sodium fluoride on reproductive function in female rats. Food Chem. Toxicol. 56, 297–303.
Zuo, H., et al., 2018. Toxic effects of fluoride on organisms. Life Sci. 198, 18–24.